Waves of sumoylation support transcription dynamics during adipocyte differentiation

By

Xu Zhao[1,2], Ivo A. Hendriks[3], Stéphanie Le Gras[4,#], Tao Ye[4,#], Aurélie Nguéa P[2], Guro Flor Lien[2], Lucia Ramos-Alonso[1,2], Arne Klungland[2], Bernard Jost[4], Jorrit M. Enserink[1,5,6], Michael L. Nielsen[3] and Pierre Chymkowitch[1,2,*]

[1] Department of Biosciences, Faculty of Mathematics and Natural Sciences, University of Oslo, P.O. Box 1066 Blindern, 0316 Oslo, Norway

[2] Department of Microbiology, Oslo University Hospital, Rikshospitalet, 0372 Oslo, Norway

[3] Proteomics Program, Novo Nordisk Foundation Center for Protein Research, Faculty of Health and Medical Sciences, University of Copenhagen, Blegdamsvej 3B, 2200, Copenhagen, Denmark.

[4] Institut de Génétique et de Biologie Moléculaire et Cellulaire, CNRS UMR7104, Inserm U1258, Université de Strasbourg, Illkirch, France

[5] Department of Molecular Cell Biology, Institute for Cancer Research, The Norwegian Radium Hospital, Montebello, 0379 Oslo, Norway

[6] Centre for Cancer Cell Reprogramming, Institute of Clinical Medicine, Faculty of Medicine, University of Oslo, Oslo, Norway

[#] Equal contribution

[*] Corresponding author: Pierre Chymkowitch

Department of Biosciences, Faculty of Mathematics and Natural Sciences, University of Oslo, P.O. Box 1066 Blindern, 0316 Oslo, Norway

Tel.: 0047-91-63-12-31

E-mail: pierre.chymkowitch@ibv.uio.no

Abstract

Tight control of gene expression networks required for adipose tissue formation and plasticity is essential for adaptation to energy needs and environmental cues. However, little is known about the mechanisms that orchestrate the dramatic transcriptional changes leading to adipocyte differentiation. We investigated the regulation of nascent transcription by SUMO during adipocyte differentiation using SLAMseq and ChIPseq. We discovered that SUMO has a dual function in differentiation; it supports the initial downregulation of pre-adipocyte-specific genes, while it promotes the establishment of the mature adipocyte transcriptional program. By characterizing sumoylome dynamics in differentiating adipocytes by mass spectrometry, we found that sumoylation of chromatin modifiers and specific transcription factors like Pparγ/RXR promotes the transcription of adipogenic genes. Our data demonstrate that the sumoylation pathway coordinates the rewiring of transcriptional networks required for formation of functional adipocytes.

Introduction

Posttranslational modification by the small ubiquitin-like modifier SUMO is a conserved, essential and versatile process playing a critical yet poorly understood role in cell differentiation, identity, growth and adaptation to various stimuli (Chymkowitch et al., 2015b; Enserink, 2015; Seeler and Dejean, 2017). Mammals express three major SUMO isoforms: SUMO-1, -2 and -3. SUMO-2 and SUMO-3 are virtually identical and usually referred to as SUMO-2/3. SUMO precursors are matured by SUMO-specific proteases (SENPs) and linked to an E1 activating enzyme. SUMO is then transferred to the E2 conjugating enzyme Ubc9, which is sufficient for conjugating SUMO to lysine residues of target proteins and which can be facilitated by E3 ligases. Sumoylation alters the stability, conformation, interactions, or subcellular localization of target proteins. SUMO targets can be desumoylated by SENPs (Chymkowitch et al., 2015b).

Proteomic studies have shown that most SUMO targets are involved in chromatin regulation, chromosome integrity, mRNA processing and transcription (Hendriks et al., 2018; Hendriks and Vertegaal, 2016). Consistently, genome-wide chromatin immunoprecipitation-sequencing (ChIPseq) experiments revealed that SUMO is present at intragenic regions, enhancers and transcription factor binding sites (Chymkowitch et al., 2015a; Chymkowitch et al., 2017; Cossec et al., 2018; Neyret-Kahn et al., 2013). The SUMO chromatin landscape is substantially remodeled in response to heat shock, inflammation, oncogene-induced senescence, nutrient deprivation and pro-growth signals (Chymkowitch et al., 2015a; Chymkowitch et al., 2017; Decque et al., 2016; Neyret-Kahn et al., 2013; Nguea et al., 2019; Niskanen et al., 2015). Recent studies have revealed that SUMO is also important for cellular identity (Cossec et al., 2018; Theurillat et al., 2020). However, these studies only compared undifferentiated versus terminally differentiated cells, precluding the sumoylation dynamics that may occur throughout the differentiation process. Therefore, there exists a need for a biologically relevant model to study sumoylome dynamics during differentiation.

Interestingly, Sumo-1 but also Senp2 knockout (KO) mice are resistant to high fat diet (HFD)-induced obesity (Mikkonen et al., 2013; Zheng et al., 2018) and white adipose tissue (WAT)-specific UBC9 KO triggers lipoatrophy (Cox et al., 2020). Consistently, loss of Sumo-1, Ubc9, Senp1 or Senp2 in cellular models impedes adipogenesis and the expression of genes under the control of PPARγ,

cEBPα, or cEBPδ, as well as genes involved in lipid and energy metabolism (Chung et al., 2010; Cignarelli et al., 2010; Liu et al., 2014). This suggests that formation of adipose tissue depends on the sumoylation pathway, although the dynamics and underlying mechanisms are poorly defined.

In this study, we used adipocyte differentiation (AD) as a model system to uncover the dynamics of the sumoylome, the SUMO-chromatin landscape and SUMO-dependent gene transcription during differentiation. Our data show that SUMO plays a dual role during adipogenesis by repressing the transcription of pre-adipocyte genes and promoting adipogenic genes transcription to establish adipocyte identity.

Results and Discussion

Sumoylation inhibition triggers lipoatrophy

To investigate the role of the sumoylation pathway during adipogenesis (AD) we differentiated mouse 3T3-L1 cells into adipocytes either in presence of DMSO or the SUMO E1 inhibitor ML-792 (He et al., 2017)(Fig. S1A). Seven days after adipogenic induction there was a normal accumulation of lipid droplets (LD) in DMSO-treated cells (Fig. S1B). In contrast, treatment with ML-792 resulted in lipoatrophy (Fig. S1B), which was characterized by numerous small LDs (Fig. S1C-D), mirroring the recently reported phenotype of Ubc9 KO in mouse white adipose tissue (Cox et al., 2020). Given that sumoylation mostly targets nuclear proteins involved in chromatin and gene regulation (Cossec et al., 2018; Hendriks et al., 2018), we hypothesized that ML-792 treatment induces lipoatrophy due to abnormalities in adipogenic gene expression programs.

Stage-specific gene expression modules of adipocyte differentiation

To investigate the role of SUMO in regulating gene expression programs during AD we assessed total RNA levels at different days of AD using QuantSeq (Herzog et al., 2017) (Fig. 1A). Principle component analysis (PCA) revealed considerable changes in total RNA levels between time points (Fig. S1E), which was further confirmed by the identification of 9426 differentially expressed genes (DEGs)(Fig. S1F and Table S1). Hierarchical clustering revealed gene expression modules with highest expression in pre-adipocytes (PA 1-3) or in mature adipocytes (MAs)(MA 7-8). We also identified gene expression modules showing either very high or very low expression during clonal expansion (CE 4-6) (Fig. S1G-H and Table S2). Although pathway enrichment did not show a single/strong function for each specific cluster, the known adipogenic inhibitors *KLF3* and *KLF10* (Garcia-Nino and Zazueta, 2021) were downregulated upon induction (Fig. S1I and J). CE modules were specifically enriched for genes involved in mitotic cell cycle regulation and adipogenesis, such as *TOP2A* and *KLF5* (Garcia-Nino and Zazueta, 2021)(Fig. S1I and J). Finally, MA modules contained genes encoding specific adipogenesis markers, like *PPARG* and *ADIPOQ* (Fig. S1I and J). With these data we characterized total mRNA dynamics during various stages of adipogenesis (Shah et al., 2014).

Mapping the nascent transcriptome landscape of differentiating adipocytes

Although we observed clear differences in RNA levels at various stages of AD, delicate changes in gene expression levels can be obscured by the large pool of background RNA. Therefore, we used SLAMseq (Herzog et al., 2017) to increase the temporal resolution of differential expression of nascent RNA during AD (Fig. 1A). PCA revealed strong transcriptional differences between day −2, day 1, and day 3, whereas day 7 showed transcriptional levels similar to day 3 (Fig. S1K). This indicates that most of the transcriptional regulation during AD is happening until day 3, while transcriptional output in mature adipocytes is stable. In total we identified 3705 DEGs (Fig. S1F and Table S3). Surprisingly, when compared to QuantSeq, SLAMseq data showed a severe and global repression of transcription upon adipogenic induction (Fig. 1B-D). Comparison of common DEGs between SLAMseq and Quantseq (Fig. S1L) revealed that this transcriptional shutdown translated into a drop of mRNA levels after day 3 (Fig. S1M). Remarkably, these repressed genes included strong adipogenic genes such as *CEBPB* and *CEBPD*, but not *CEBPA* (Fig. 1E and S1H and N). This indicates that although transcriptional repression of many genes is required at induction, many mRNAs remain available for several days. This emphasizes unforeseen discrepancies between total RNA levels and transcription rates during adipogenesis.

Hierarchical clustering revealed that a vast majority of genes (3433; modules 1-4 and 6-8) were transcribed in PA stage and then downregulated upon adipogenic induction (Fig. 1D-E). Transcription of these genes, including anti-adipogenic *KLF3* and *KLF10*, reached minimum levels either during CE or at MA stage (Fig. 1E-F and Table S4). On the other hand, a comparatively small number of genes (273) displayed increased transcription upon adipogenic induction (Fig. 1D-E). Among those, only transcription module 5 contained genes highly transcribed during CE, which included *TOP2A* and *KLF5* (Fig. 1D-F and Table S4). Finally, transcription modules 9-11 contained genes highly expressed in MAs, such as *PPARG* and *ADIPOQ* (Fig. 1D-F and Table S4).

Contrary to QuantSeq, pathway enrichment analysis of SLAMseq data revealed a partial overlap between terms in PA and CE (Fig. 1G and S1I). These terms included mitotic regulation of the cell cycle (Fig. 1G), indicating that transcriptional regulation of cell cycle events of CE is occurring very shortly

after adipogenic induction. In the SLAMseq data, MA-specific transcription modules 9-11 demonstrated a very strong enrichment in genes involved in fat cell differentiation and mature adipocyte functions, including triglyceride metabolism, glucose homeostasis, and lipid storage (Fig. 1G). Thus, we conclude that adipogenic induction triggers i) transcriptional downregulation of most of the genes that are transcribed in pre-adipocytes, including some adipogenic genes; and ii) upregulation of strongly pro-adipogenic genes, which reach maximum transcriptional output in MAs (Fig. 1D).

SUMO promotes transcription of pro-adipogenic genes

Next, we studied the effect of sumoylation on the transcriptional landscape of differentiating 3T3-L1 cells by treating cells with ML-792 (Fig. 2A). Differential expression analysis of ML-792 versus DMSO control samples revealed 5833 QuantSeq DEGs (9561 transcripts; Table S5) and 905 SLAMseq DEGs (1334 transcripts; Table S6) (Fig. S1F). Whereas QuantSeq analysis did not detect significant effects of ML-792 over time (Fig. 2B), SLAMseq revealed significant and global downregulation of transcription at days 1 and 7 and upregulation at day 3 (Fig. 2C). Pathway enrichment analysis revealed that these DEGs are involved in various processes, most notably regulation of fat cell differentiation (Fig. 2D and Fig. S2A). Interestingly, hierarchical clustering revealed that ML-792 affected the transcription of many genes during adipogenesis (Fig. 2E, Fig. S2B and Table S7). These data show that sumoylation is important for establishing adipocyte transcription programs.

We then investigated whether sumoylation is specifically important either for maintaining transcription patterns over time (Fig. 2F, *left insert*) or for regulation of overall transcriptional amplitude (Fig. 2F, *right insert*) during AD. ML-792 only had a limited effect on overall transcription patterns (Fig. 2F, for an example see *MT2* in Fig. 2G, *upper panel*). In contrast, it strongly affected the transcriptional amplitude of a large number of genes (Fig. 2F), such as *SCD1* (Fig. 2G, *lower panel* and S4K). Expanding this analysis to the AD stage-specific transcription modules identified in Fig. 1D, we discovered that ML-792 treatment primarily affected transcription amplitude in all modules, whereas it affected both pattern and amplitude of MA-specific modules 9-11 (Fig. S2C-D). This indicates a more profonde effect of ML-792 on transcription of adipocyte genes. More specifically, ML-792 treatment resulted in downregulation of MA-specific genes involved in fat cell differentiation starting from day 1

after adipogenic induction, while transcription of an equal number of randomly selected genes or steady state mRNA levels were not affected (Fig. 2H, Fig. S2E and Table S8).

Together, these data indicate that sumoylation is particularly important for sustaining high transcription levels of genes involved in fat cell differentiation and adipogenic function.

Chromatin-bound SUMO promotes the transcriptional identity switch from pre-adipocyte to mature adipocyte

To gain insight into the dynamics and location of SUMO at chromatin during AD we performed ChIPseq experiments using an anti Sumo-2/3 antibody (Fig. 3A). PCA revealed good correlation between biological replicates and strong variation between time points (Fig. S3A). We identified 35,659 SUMO peaks (Table S9), which were primarily located at transcription units, especially at promoters (Fig. S3B). Strikingly, both the number and intensity of SUMO peaks increased after induction of adipogenesis (Fig. 3B). Pathway enrichment analysis showed that SUMO peaks are overrepresented at genes involved in fat cell differentiation and genes with hallmark MA functions, such as lipid metabolism (Fig. S3C).

Hierarchical clustering identified SUMO binding modules with highest ChIP signals at PA, CE and MA stages (Fig. 3C-D and Table S10). PA modules 1-4 contained 544 SUMO peaks of which the intensity decreased upon adipogenic induction. These peaks were assigned to a heterogeneous set of genes that did not show significant pathway enrichment (Fig. 3E). The same was observed for CE modules 5-7 that contained 170 peaks with highest intensity at day 1 or 3 (Fig. 3E). Finally, MA modules 8-12 contained 1136 peaks with highest intensity in MAs and a very strong enrichment for genes involved in adipogenic functions as well as adaptive thermogenesis (Fig. 3E). These data indicate that chromatin-bound SUMO supports adipocyte function and metabolism via transcriptional regulation.

By integrating the SLAMseq transcription modules identified in Fig. 1D with SUMO ChIPseq data, followed by hierarchical clustering, we found that distinct peaks of SUMO were present both at repressed genes and at activated genes upon induction of adipogenic differentiation (Fig. 3F-G and Table S11). Pearson scoring revealed a general positive correlation between transcription and the presence of SUMO (Fig. 3H-I). This was especially true for exons, introns and distant promoters. However, the

presence of SUMO at promoter regions strongly anticorrelated with transcription (Fig. 3H), and most PA genes appear to be inhibited by the presence of SUMO at the promoter upon induction of adipogenic differentiation (Fig. 3I), such as the AD inhibitor *KLF10* (Fig. S3D). In clear contrast, the presence of SUMO at MA gene promoters showed almost exclusively a positive correlation with transcription (Fig. 3I), such as the adipogenic gene *FABP4* (Fig. S3D).

Based on these findings, we hypothesized that adipogenic stimulation leads to increased sumoylation of transcription factors to inhibit transcription of PA genes while increasing transcription of MA genes. We integrated ML-792 SLAMseq data with CTRL SLAM-seq and ChIPseq datasets by hierarchical clustering (Fig. S3E and Table S12). This revealed two main categories of SUMO-target genes independently of whether they are activated or repressed upon adipogenic induction: Genes at which SUMO functions as a corepressor, and genes where it serves as a coactivator (Fig. 3J-K and Table S13). Generally, genes activated by SUMO are involved in fat cell differentiation and carbohydrate metabolism, whereas genes repressed by SUMO are not related with adipogenesis (Fig. S3F).

We conclude that (i) chromatin-bound SUMO has a dual role during AD by repressing PA genes while promoting MA genes; and (ii) that SUMO plays an instrumental role in the transcriptional identity switch from pre-adipocyte to mature and functional adipocyte.

Waves of SUMO on chromatin upon induction of adipogenic differentiation

To identify potential transcription factor binding sites (TFBS) enriched for SUMO, we performed a motif search using the SUMO ChIPseq dataset as input (Table S14). While no TFBS for adipogenic factors was retrieved at day −2 (Fig. 3L and S3G), we observed significant recruitment of SUMO at critical adipogenic TFBSs over time after stimulation of adipogenic differentiation (Fig. 3L and Fig. S3G). A first wave of SUMO was detected at Cebpβ, GR and Atf4 TFBSs shortly after adipogenic induction from day 1 until day 7. A second wave of SUMO occurred at Pparγ and RXR response elements, starting on day 3 and lasting until day 7. Similar results were obtained with TFBS analysis of SUMO peaks that are found at AD-regulated genes identified in the SLAMseq dataset (Fig. S3H). To validate these findings, we integrated our SUMO ChIPseq data with published

Pparγ/RXR ChIPseq (Nielsen et al., 2008). Strikingly, there was a very significant and progressive timely overlap between SUMO, Pparγ and RXR peaks during AD (Fig 3M and S4K and Table S15).

These data show that the increase in SUMO binding to genes that are regulated during AD occurs at very specific adipogenic TFBS like Cebpβ, GR and Pparγ/RXR. Importantly, SUMO recruitment to Pparγ/RXR TFBSs follows the known timeline of recruitment of these TFs during AD (Lefterova et al., 2014; Nielsen et al., 2008).

Site-specific characterization of the SUMOylome during adipocyte differentiation

To identify adipogenesis-specific SUMO2 substrates we carried out site-specific characterization of the endogenous SUMOylome by mass spectrometry during AD (Fig. 4A)(Hendriks et al., 2018). PCA of SUMO-modified lysine residues of four independent experiments demonstrated high reproducibility between replicates and considerable differences between the time points (Fig. S4A-B). Across all time points, fractions and biological replicates, we identified 5230 SUMO-modified peptides that mapped to 3706 unique SUMO sites. Out of all SUMO sites, 3137 (~85%) could be quantified in quadruplicate (Table S16).

In accordance with SUMO western blots (Fig. S4C), MS experiments showed that the overall density of SUMO increases upon adipogenic induction (Fig. 4B). Furthermore, when we analyzed the SUMO equilibrium, i.e. the distribution of SUMO across the entire system and whether it exists in a free or in a conjugated form, we found a larger portion of immature as well as free SUMO prior to induction of differentiation (Fig. 4C). Upon adipogenic induction the demand for and usage of SUMO went up to reach near-maximum levels at the later time points (Fig. 4C), which coincided with the sharp and sustained increase of SUMO binding to the chromatin observed in Fig. 3. In total, we identified 1389 SUMO target proteins of which 1156 could be quantified in quadruplicate with high reproducibility (Table S17, Suppl. Fig. S4D). Pathway enrichment analysis showed that these targets are involved in chromatin regulation, transcription, chromosome maintenance, and cell cycle progression (Fig. S4E and Table S18). This is consistent with previous reports (Hendriks et al., 2018; Theurillat et al., 2020), although a unique aspect of our study is the specific enrichment of pathways

that are critical for adipose tissue development, function, adaptive thermogenesis, and brown cell differentiation (Fig. S4E-G).

Hierarchical clustering of the SUMO targets further underlined the sharp remodeling of the SUMOylome occurring after adipogenic induction (Fig. 4D and Table S19). Only very few (21) proteins were highly sumoylated at PA stage; a notable example being the transcriptional repressor Zbtb4 (Fig. 4E and Fig. S4H). However, 174 out of 1250 SUMO targets were highly sumoylated during CE (Fig. 4E). These proteins are involved in mitotic chromosome maintenance or in nucleosome modification, and include Top2A, CdcA5, CBP/p300, Hdac2 and Hdac4 (Fig. 4E-F and Fig. S4H). Interestingly, the 1055 MA-specific targets were enriched for proteins critical for fat cell differentiation (Fig. 4F). These targets include pro-adipogenesis TFs like GR, cEBPα/δ, Pparγ and RXR, but also proteins involved in fat metabolism, such as Fabp4 or FasN (Fig. 4E, Fig. S4H). This strongly suggests that the timely sumoylation of proteins during CE and MA stages supports mitotic events, fat cell differentiation and adipogenic function in mature adipocytes.

Sumoylation supports transcription in mature adipocytes

Our data indicate that the SUMO peaks detected at GR, cEBPδ and Pparγ/RXR binding sites (Fig. 3 and S3) are due to the presence of sumoylated TFs. Therefore, we integrated the SUMO MS, SUMO SLAMseq, SUMO ChIPseq, and Pparγ/RXR ChIPseq datasets and focused on Pparγ/RXR target genes of which the regulation is critical during AD (Nielsen et al., 2008). We identified 208 genes at which SUMO perfectly overlapped with Pparγ/RXR (Figure 4G and Table S20). Note that these genes are adipogenic genes (Fig. S4I) that are either repressed (PA genes) or activated (MA genes) by adipogenic stimulation (Fig. 4H and S4J). Pparγ/RXR became sumoylated upon adipogenic induction, which was shortly followed by an increased presence of SUMO at Pparγ/RXR response elements (Fig. S4J *and example of SCD1 gene in Fig S4K*). This correlated with repression of PA genes and activation of MA genes, underscoring the dual role of SUMO in transcriptional regulation. Importantly, ML-792 led to the downregulation of PA genes and upregulation of MA genes at day −2 whereas MA genes, were strongly downregulated at day 7 (Fig. 4H-I and S4J-K).

These data indicate that the timely regulation of Pparγ/RXR target genes in response to adipogenic stimulation requires the activity of the sumoylation pathway. Inhibiting the sumoylation process perturbed the transcription of these genes and did not allow for development of proper adipogenic functions, which resulted in lipoatrophy (Fig. S1B and 4I). Understanding the exact molecular mechanisms by which sumoylation regulates transcription factors such as Pparγ/RXR will be the scope of our follow-up studies. Based on previous work by ourselves and others, sumoylation may affect chromatin accessibility (repressive versus permissive), DNA binding capacity or stability of chromatin-bound transcriptional complexes (Chymkowitch et al., 2015a; Chymkowitch et al., 2017; Cossec et al., 2018; Psakhye and Jentsch, 2012; Theurillat et al., 2020).

Taken together, we have shown that adipogenesis involves a robust increase of SUMO at transcription units, and that SUMO is important for the establishment and robustness of adipogenic transcription programs to enforce the identity shift from pre-adipocyte to mature adipocyte.

STAR methods

Lead Contact

Further information and requests for resources and reagents should be directed to and will be fulfilled by the corresponding author Pierre Chymkowitch (pierre.chymkowitch@ibv.uio.no).

Materials Availability

This study did not generate new unique reagents.

Data and code availability

The SLAMseq / Quantseq and SUMO ChIPseq datasets data have been deposited to the Gene Expression Omnibus.

The accession numbers for published PPARγ and RXR ChIPseq data are GSM340795, GSM340796, GSM340799, GSM340801, GSM340802 and GSM340805 (Nielsen et al., 2008).

The mass spectrometry proteomics data have been deposited to the ProteomeXchange Consortium via the PRIDE partner repository with the dataset identifier PXD024144.

EXPERIMENTAL MODEL AND SUBJECT DETAILS

3T3-L1 culture, differentiation and treatments

3T3-L1 preadipocytes (CL-173, ATCC) were maintained in Dulbecco's modified Eagle's medium (DMEM) supplemented with 10% bovin calf serum (12138C, Sigma) and 1 % Penicillin/Streptavidin (P/S) at 37 °C in a humidified incubator in a 5 % CO_2 in air atmosphere. Before adipogenic induction 3T3-L1 preadipocytes were grown to confluence by replacing the maintenance medium every second day for at least 4 days. Differentiation of 3T3-L1 cells was induced with differentiation medium (DMEM supplemented with 10 % fetal bovine serum (F7524, Sigma), 1mM dexamethasone (D4902, Sigma), 0.5 mM 3-isobutyl-1-methylxanthine (I5879, Sigma), 10 µg/mL insulin and 1 % P/S). At day 3 post adipogenic induction, the differentiation medium was replaced with the adipocyte maintenance medium (DMEM supplemented with 10 % FBS, 10 µg/mL of insulin and 1 % P/S). Adipocyte maintenance medium was then refreshed every second day.

SUMOylation was inhibited by supplementing the culture medium with 0.5 µM of ML-792 (407886, Medkoo Biosite).

METHOD DETAILS

Lipid droplet staining

3T3-L1 cells were grown as described in "Adipocyte culture, differentiation and treatment". At day 7 post induction cells were washed with PBS and fixed with 4.5 % formaldehyde during 10 minutes and rinsed 3 times with PBS. Lipid droplets were stained with a Bodipy 493/503 (D3922, Thermo Fisher Scientific) staining solution (1 µg/mL Bodipy 493/503, 150 mM NaCl) for 10 min at room temperature. Nuclei were stained with DAPI (0.5 µg/mL).

Image acquisition

Images were acquired using the ImageXpress Micro Confocal device (Molecular devices, serial number 5150066). Widefield images were acquired using the 40 X S Plan Fluor ELWD objective as Z-series (step sizes 0.2-1 µm, depending on the staining). At least 4 representative fields per well were captured.

Image analysis and quantification

All images were analyzed using the FIJI software (Fiji is just ImageJ) (National Institutes of Health, Bethesda, MD, USA). Z series images were corrected from bleaching then projected to obtain a "focused" single image corresponding to the different focal planes, using the *Stack Focuser* plugin (https://imagiej.nih.gov/ij/plugins/stack-focuser.html). Lipid droplets were segmented and quantified in single cell using the *Lipid Droplets Tool* macro (http://dev.mri.cnrs.fr/projects/imagej-macros/wiki/Lipid_Droplets_Tool) (Colitti et al., 2018).

QuantSeq and SLAM-Sequencing sample preparation

3T3-L1 cells were grown as described in "*Adipocyte culture, differentiation and treatment*" and treated with DMSO or ML-792. Three biological replicates were harvested per condition. Prior

harvesting, nascent RNAs were labelled with 100 µM of 4-thiouridine during 45 min. After labelling cells were lysed, homogenized and collected using 1 ml of RNAzol®RT (RN190-100, Molecular Research Center) before adding 0.4 ml of water per 1 ml of homogenate. The mixture was vortexed for 5 min and centrifuged at 12,000 g for 15 min. Following centrifugation, DNA, proteins and polysaccharides form a semisolid pellet at the bottom of the tube. The RNA remains soluble in the supernatant. The supernatant (1 ml maximum) was transferred to a new tube and 1 volume of 70% ethanol was added. The mixture was homogenized by pipetting (do not centrifuge). Samples were then applied to a RNeasy spin column (74104, Qiagen) and RNAs were purified according to Qiagen's instructions. Base conversion was performed using the SLAMseq catabolic kinetics module (Lexogen, 062.24). RNA quantification and quality control were performed using Tape Station 4150 (Agilent).

Library preparation and sequencing of QuantSeq and SLAMseq samples

mRNA-Seq libraries were generated according to manufacturer's instructions from 500 ng of total RNA using the QuantSeq 3′mRNA-Seq Library Prep Kit for Illumina (FWD) (# 015, Lexogen GmbH, Vienna, Austria). Reverse transcription was initiated by oligo dT priming. After first strand cDNA synthesis the RNA was removed and second strand synthesis was initiated by random priming. Oligo dT primer and random primers contain Illumina-compatible adapter sequences. The resulting double-stranded cDNA was then purified and PCR amplified (30 sec at 98°C; [10 sec at 98°C, 20 sec at 65°C, 30 sec at 72°C] x 11 cycles; 1 min at 72°C), introducing i7 indexes. Surplus PCR primers were further removed by purification using SPRI-select beads (Beckman-Coulter, Villepinte, France) and the final libraries were checked for quality and quantified using capillary electrophoresis. The libraries were sequenced on Illumina Hiseq 4000 sequencer as Single-Read 50 base reads following Illumina's instructions. Image analysis and base calling were performed using RTA 2.7.7 and bcl2fastq. 2.17.1.14. Adapter dimer reads were removed using DimerRemover (https://sourceforge.net/projects/dimerremover/).

SLAMseq and QuantSeq data analysis

mm10 mouse genome assembly and Refseq 3'UTR coordinates were downloaded from UCSC (4 August 2020) using Table Browser. Sequencing reads were mapped and filtered with SlamDunk pipeline v0.4.3 (http://t-neumann.github.io/slamdunk/docs.html #document-Dunks). SlamDunk all (http://t-neumann.github.io/slamdunk/docs.html#all) was applied to full analysis for all samples. Reads with ≥ 1 T>C conversions were considered as labeled reads. Default settings for other parameters was followed.

Two parallel differential gene expression analyses were performed using DESeq2 R package (1.26.0). The total RNA reads were used for Quantseq analysis. The normalization size factor in Quantseq analysis was applied to global normalization for labeled reads. Time course experiments design (http://master.bioconductor.org/packages/release/workflows/vignettes/rnaseqGene/inst/doc/rnaseqGene.html#time-course-experiments) was adapted for our data. Principal component analysis was performed after variance stabilizing transformation on total genes for both analyses.

Chromatin immunoprecipitation (ChIP)

3T3-L1 cells were grown as described in "*Adipocyte culture, differentiation and treatment*" in 15 cm dishes. Two dishes were used per biological replicate and two biological replicates were collected for each time point.

Our ChIP procedure was adapted from (Baik et al., 2018). Cells were cross-linked in dish with 1% formaldehyde for 8 minutes. Formaldehyde was then neutralized using 125 mM glycine for 10 minutes. After two washes with cold PBS the cells were collected in the Lysis buffer (5 mM PIPES pH 7.5, 85 mM KCl, 0.5% NP40, 20 mM N-ethyl maleimide [NEM] and protease inhibitor cocktail [04693159001, Roche]) and incubated at 4°C for 10 minutes with rotation. Nuclei were centrifuged (1,500 rpm for 10 minutes at 4°C) and resuspended in a nucleus lysis buffer (50 mM Tris-HCl pH 7.5, 1% SDS, 10 mM EDTA, 20 mM NEM and protease inhibitor cocktail) and incubated at 4°C for 2 hours. Lysates were sonicated for 15 cycles (30 sec on / 30 sec off) at 4°C using a Bioruptor Pico sonicator (Diagenode). After sonication, lysates were centrifuged at 14,000 rpm for 10 minutes at 4°C. Protein concentration was assessed using the Bradford assay and 250 µg of chromatin were used for each immunoprecipitation. Input samples (12.5 µg) were saved. Samples were diluted 10-fold in the

immunoprecipitation buffer (1.1% Triton X100, 50 mM Tris-HCl pH 7.5, 167 mM NaCl, 5 mM N-ethyl maleimide, 1 mM EDTA, 0.01% SDS, and protease inhibitor cocktail). Immunoprecipitations were carried out with 10 µg of SUMO-2/3 antibody (ab3742, Abcam) and 420 µl of Dynabeads Protein A (10001D, Thermo Fisher Scientific) overnight at 4°C. Beads were then washed 2 times in low-salt buffer (50 mM Tris-HCl pH 7.5, 150 mM NaCl, 1% Triton X100, 0.1% SDS, 1 mM EDTA), 2 times in high-salt buffer (50 mM Tris-HCl pH 7.5, 500 mM NaCl, 1% Triton X100, 0.1% SDS, 1 mM EDTA), 2 times in LiCl buffer (20 mM Tris-HCl pH 7.5, 250 mM LiCl, 1% NP40, 1% deoxycholic acid, 1 mM EDTA) and in TE buffer (10 mM Tris-HCl pH 7.5, 0.2% Tween20, 1 mM EDTA). Elution was done two time in 50 µL of 100 mM NaHCO3, 1% SDS at 65°C for 10 min under agitation. Chromatin cross-linking was reversed at 65°C for 5 hours with 280 mM NaCl and 88 µg/mL RNase DNase free (11119915001, Roche). Proteins were then digested using 88 µg/mL of Proteinase K (03115828001, Roche) during 1 hour at 65°C. DNA from immunoprecipitations and inputs were purified using the Qiagen PCR purification kit. DNA concentration was assessed using a Qubit device (Q32866, Invitrogen).

Library preparation and sequencing of ChIP samples (ChIP-seq)

ChIP samples were purified using Agencourt AMPure XP beads (Beckman Coulter) and quantified with the Qubit (Invitrogen). ChIP-seq libraries were prepared from 10 ng of double-stranded purified DNA using the MicroPlex Library Preparation kit v2 (C05010014, Diagenode s.a., Seraing, Belgium), according to manufacturer's instructions. In the first step, the DNA was repaired and yielded molecules with blunt ends. In the next step, stem-loop adaptors with blocked 5 prime ends were ligated to the 5 prime end of the genomic DNA, leaving a nick at the 3 prime end. The adaptors cannot ligate to each other and do not have single-strand tails, avoiding non-specific background. In the final step, the 3 prime ends of the genomic DNA were extended to complete library synthesis and Illumina compatible indexes were added through a PCR amplification (7 cycles). Amplified libraries were purified and size-selected using Agencourt AMPure XP beads (Beckman Coulter) to remove unincorporated primers and other reagents. The libraries were sequenced on Illumina Hiseq 4000 sequencer as Single-Read 50 base reads following Illumina's instructions. Image analysis and base

calling were performed using RTA 2.7.7 and bcl2fastq 2.17.1.14. Adapter dimer reads were removed using DimerRemover.

ChIP-seq sequencing data analysis

Reads were mapped to the Mus musculus genome (assembly mm10) using Bowtie (Langmead, 2010) v1.0.0 using the following parameters -m 1 --strata --best. Reads mapped in genomic regions flagged as ENCODE blacklist were removed (Amemiya et al., 2019). SUMO peaks were called with the ENCODE ChIP-seq pipeline v1.3.6. Briefly, the pipeline ran quality controls and called peaks with spp v1.15.5 (Kharchenko et al., 2008). Reproductible peaks were kept after the IDR analysis was run (optimal IDR sets of peaks were kept). Peaks were annotated relative to genomic features using Homer annotatePeaks.pl v4.11.1 (Heinz et al., 2010). Known or *de novo* TF motifs were identified using HOMER findMotifsGenome.pl with default parameters. Heatmaps and mean profiles presenting read enrichments at various genomic locations were generated using Easeq software v1.111 (Lerdrup et al., 2016). To compare SUMO peaks enrichments over time, the union of all peak positions was computed with BEDtools v2.26.0 (Quinlan and Hall, 2010). Then, read counts per peak (union peak set) were normalized across libraries with the method proposed by Anders and Huber (Anders and Huber, 2010) and implemented in the Bioconductor package v1.24.0 (Love et al., 2014). Regions varying due to time effect were identified using a likelihood ratio test (LRT) with DESeq2. Resulting p-values were adjusted for multiple testing using the Benjamin and Hochberg method (Benjamini and Hochberg, 1995). Significant regions were those which adjusted p-value ≤ 0.05, absolute fold change > 1.5.

RXR and Pparγ ChIP-seq datasets

RXR and Pparγ data were mapped to the Mus musculus genome (assembly mm10) using Bowtie (Langmead, 2010) v1.0.0 using the following parameters -m 1 --strata –best. Peaks were called using MACS2 callpeak with default parameters except for -g mm --nomodel --extsize 200. Peaks were annotated relative to genomic features using Homer annotatePeaks.pl v4.11.1 (Heinz et al., 2010).

	Time	Cells	Type	GEO accession	Reference
Pparγ	Day 1	3T3L1	ChIP-seq	GSM340795	(Nielsen et al., 2008)
Pparγ	Day 2	3T3L1	ChIP-seq	GSM340796	(Nielsen et al., 2008)
Pparγ	Day 6	3T3L1	ChIP-seq	GSM340799	(Nielsen et al., 2008)
RXR	Day 1	3T3L1	ChIP-seq	GSM340801	(Nielsen et al., 2008)
RXR	Day 2	3T3L1	ChIP-seq	GSM340802	(Nielsen et al., 2008)
RXR	Day 6	3T3L1	ChIP-seq	GSM340805	(Nielsen et al., 2008)

SUMO Mass Spectrometry

3T3-L1 cells were grown as described in "*Adipocyte culture, differentiation and treatment*". Four biological replicates were collected for each condition. Cells were washed with PBS supplemented with 20 mM NEM (E3876, Merck Life Science). Cells were vigorously lysed in guanidium lysis buffer (6M guanidine-HCl, 50 mM Tris pH 8.5, 20 mM NEM), after which they were immediately snap frozen. Lysates were stored at −80°C until further processing. In essence, sample preparation and SUMO-IP for native and endogenous mass spectrometry (MS) analysis was performed as described previously (Hendriks et al., 2018). Lysates were thawed at room temperature, after which they were supplemented with 5 mM chloroacetamide (CAA) and 5 mM Tris(2-carboxyethyl)phosphine (TCEP). Samples were homogenized via sonication using a microtip sonicator, at 30 W using three 10 s pulses, and afterwards cleared by centrifugation at 4,250*g*. Endoproteinase Lys-C (Wako) was added to samples in a 1:200 enzyme-to-protein ratio (w/w). Digestion was performed overnight, still, and at room temperature. Digested samples were diluted with three volumes of 50 mM ammonium bicarbonate (ABC), and a second round of overnight digestion was performed by addition of Lys-C in a 1:200 enzyme-to-protein ratio. Digests were acidified by addition of 0.5% trifluoroacetic acid (TFA), 1:100 vol/vol from a 50% TFA stock, after which they were transferred to 50 mL tubes and centrifuged at 4,250*g* and at 4°C for 30 min. Clarified digests were carefully decanted into clean 50 mL tubes, after which peptides were purified using C8 Sep-Pak cartridges (Waters) according to the manufacturer's instructions. Sep-Pak cartridges with 500

mg C8 sorbent were used, with one cartridge used for each ~25 mg of digested protein. Small and hydrophilic peptides were pre-eluted using 5 mL of 20% acetonitrile (ACN) in 0.1% TFA, and 3 mL of 25% ACN in 0.1% TFA. SUMOylated peptides were eluted using 1 mL of 35% ACN in 0.1 TFA, 1 mL of 40% ACN in 0.1% TFA, and 2 mL of 45% ACN in 0.1% TFA. For each replicate sample, all SepPak elutions were pooled in 50 mL tubes with small holes punctured into the caps, and then frozen overnight at −80°C. Deep-frozen samples were lyophilized to dryness for 48 h, with the pressure target set at 0.004 mbar and the condenser coil at −85°C.

Crosslinking of SUMO antibody to beads

Overall, 750 µL of Protein G Agarose beads (Roche) were used to capture 400 µL of SUMO-2/3 antibody (8A2, acquired from Abcam, ab81371; ~5-10 µg/µL antibody). All washing and handling steps were followed by centrifugation of the beads at 500*g* for 3 min in a swing-out centrifuge with delayed deceleration and careful aspiration of buffers, to minimize loss of beads. Beads were pre-washed 4 times with ice-cold PBS, split across three 1.5 mL tubes, after which the antibody was added and the tubes filled completely with ice-cold PBS. Beads and antibody were incubated at 4°C on a rotating mixer for 1 h, and subsequently washed 3 times with ice-cold PBS. Crosslinking of the antibody to the beads was achieved by addition of 1 mL of 0.2 M sodium borate, pH 9.0, which was freshly supplemented with 20 mM dimethyl pimelimidate (DMP). Crosslinking was performed for 30 min at room temperature on a rotating mixer, after which the crosslinking step was repeated once. SUMO-IP beads where then washed twice with ice-cold PBS, twice with 0.1 M glycine pH 2.8, and three times with ice-cold PBS, after which all beads were pooled in a single 1.5 mL tube and stored until use at 4°C in PBS supplemented with 10 mM sodium azide.

Purification of SUMOylated peptides

Lyophilized peptides were dissolved in 10 mL ice-cold SUMO-IP buffer (50 mM MOPS, 10 mM Na2HPO4, 50 mM NaCl, buffered at pH 7.2) per 50 mg protein originally in the samples. Samples were clarified by centrifugation at 4,250*g* for 30 min at 4°C in a swing-out centrifuge with delayed deceleration. Samples were transferred to new tubes, after which 25 µL SUMO-IP beads was added per

50 mg protein originally in the samples. Samples were incubated at 4°C for 3 h in a rotating mixer, after which the beads were washed twice with ice-cold SUMO-IP buffer, twice with ice-cold PBS, and twice with ice-cold MQ water. Upon each first wash with a new buffer, beads were transferred to a clean 1.5 mL LoBind tube (Eppendorf). To minimize loss of beads, all centrifugation steps were performed at 500*g* for 3 min at 4°C in a swing-out centrifuge with delayed deceleration. Elution of SUMO peptides from the beads was performed by addition of 2 bead volumes of ice-cold 0.15% TFA, and performed for 30 min while standing still on ice, with gentle mixing every 10 min. The elution of the beads was repeated once, and both elutions were cleared through 0.45 µm spin filters (Millipore) by centrifuging at 12,000*g* for 1 min at 4°C. The two elutions from the same samples were pooled after clarification. Next, samples were pH-neutralized by addition of 1/10th volume of 1 M Na_2HPO_4, and allowed to warm up to room temperature. Second-stage digestion of SUMOylated peptides was performed with 1 µg of Endoproteinase Asp-N (Roche). Digestion was performed overnight, at 30°C and shaking at 300 rpm, after which samples were frozen at −80°C until further processing.

StageTip purification and high-pH fractionation of SUMO-IP samples

Preparation of StageTips (Rappsilber et al., 2003), and high-pH fractionation of SUMO-IP samples on StageTip, was performed essentially as described previously (Hendriks et al., 2018). Quad-layer StageTips were prepared using four punch-outs of C18 material (Sigma-Aldrich, Empore™ SPE Disks, C18, 47 mm). StageTips were equilibrated using 100 µL of methanol, 100 µL of 80% ACN in 200 mM ammonium, and two times 75 µL 50 mM ammonium. Samples were thawed out, and supplemented with 1/10th volume of 200 mM ammonium, just prior to loading them on StageTip. The StageTips were subsequently washed twice with 150 µL 50 mM ammonium, and afterwards eluted as six fractions (F1-6) using 40 µL of 4, 7, 10, 13, 17, and 25% ACN in 50 mM ammonium. All fractions were dried to completion in LoBind tubes, using a SpeedVac for 2 h at 60°C, after which the dried peptides were dissolved using 10.5 µL of 0.1% formic acid.

MS analysis

All samples were analyzed on EASY-nLC 1200 system (Thermo) coupled to a Q Exactive™ HF-X Hybrid Quadrupole-Orbitrap™ mass spectrometer (Thermo). For each run, 5 µL of sample was injected. Separation of peptides was performed using 15-cm columns (75 µm internal diameter) packed in-house with ReproSil-Pur 120 C18-AQ 1.9 µm beads (Dr. Maisch). Elution of peptides from the column was achieved using a gradient ranging from buffer A (0.1% formic acid) to buffer B (80% acetonitrile in 0.1% formic acid), at a flow of 250 nl/min. Gradient length was 80 min per sample, including ramp-up and wash-out, and an analytical gradient of 50 min. The buffer B ramp for the analytical gradient was as follows: F1: 13-24%, F2: 14-27%, F3-5: 15-30%, F6: 17-32%. The columns were heated to 40°C using a column oven, and ionization was achieved using a Nanospray Flex Ion Source (Thermo) with the spray voltage set at 2 kV, an ion transfer tube temperature of 275°C, and an RF funnel level of 40%. Full scan range was set to 400-1,600 *m*/*z*, MS1 resolution to 60,000, MS1 AGC target to 3,000,000, and MS1 maximum injection time to 60 ms. Precursors with charges 2-6 were selected for fragmentation using an isolation width of 1.3 *m*/*z*, and fragmented using higher-energy collision disassociation (HCD) with normalized collision energy of 25. Precursors were excluded from re-sequencing by setting a dynamic exclusion of 60 s. MS2 resolution was set to 60,000, MS2 AGC target to 200,000, minimum MS2 GC target to 20,000, MS2 maximum injection time to 120 ms, and loop count to 7.

Analysis of MS data

All MS RAW data was analyzed using the freely available MaxQuant software, version 1.5.3.30 (Cox and Mann, 2008; Cox et al., 2011). All data was processed in a single computational run, and default MaxQuant settings were used, with exceptions specified below. For generation of the theoretical spectral library, the mouse FASTA database was downloaded from Uniprot on the 14th of February, 2020. The mature sequence of SUMO2 was inserted in the database to allow for detection of free SUMO. In silico digestion of theoretical peptides was performed with Lys-C, Asp-N, and Glu-N, allowing up to 8 missed cleavages. Variable modifications used were protein N-terminal acetylation, methionine oxidation, peptide N-terminal pyroglutamate, Ser/Thr/Tyr phosphorylation (STY), and Lys SUMOylation, with a maximum of 3 modifications per peptide. The SUMO mass remnant was defined

as described previously (Hendriks et al., 2018); DVFQQQTGG, $H_{60}C_{41}N_{12}O_{15}$, monoisotopic mass 960.4301, neutral loss b7-DVFQQQT, diagnostic mass remnants [b2-DV, b3-DVF, b4-DVFQ, b5-DVFQQ, b6-DVFQQQ, b7-DVFQQQT, b9-DVFQQQTGG, QQ, FQ, FQQ]. Label-free quantification was enabled, with "Fast LFQ" disabled. Maximum peptide mass was set to 6,000 Da. Stringent MaxQuant 1% FDR filtering was applied (default), and additional automatic filtering was ensured by setting the minimum delta score for modified peptides to 20, with a site decoy fraction of 2%. Second peptide search was enabled (default). Matching between runs was enabled, with a match time window of 1 min and an alignment window of 20 min. For protein quantification, the same variable modifications were included as for the peptide search. To further minimize false-positive discovery, additional manual filtering was performed at the peptide level. All modified peptides were required to have a localization probability of >75%, be supported by diagnostic mass remnants, be absent in the decoy database, and have a delta score of >40 in case SUMO modification was detected on a peptide C-terminal lysine not preceding an aspartic acid or glutamic acid. All multiply-SUMOylated peptides were discarded, unless the corresponding SUMO sites were also identified by singly-SUMOylated peptides. SUMO target proteins were derived from the "proteinGroups.txt" file, and all post-filtering SUMO sites were manually mapped. Only proteins containing at least one SUMO site were considered as SUMO target proteins, and other putative SUMO target proteins were discarded.

Calculation of SUMO density and equilibrium

SUMO density was calculated by dividing the total sum of all SUMO site intensity (in arb. units., corresponding to ion current) by the amount of total protein starting material (in mg). This calculation was performed for each replicate separately, and visualized as an average ± standard deviation. The mature sequence of SUMO2 was included as a FASTA file in the MaxQuant search, to allow detection of free mature SUMO2/3. For quantification of the SUMO equilibrium, the "modificationSpecificPeptides.txt" MaxQuant output file was used, and all peptides modified by SUMO2/3, and peptides derived from SUMO2/3 itself, were considered. Modification of any SUMO family member by SUMO 2/3 was considered chain formation, with all other conjugation considered as global target modification. Peptides derived from SUMO2/3 were sub-classed as internal, mature

free SUMO2/3, immature SUMO2, or immature SUMO3. Peptides ending in QQTGG (predominantly DVFQQQTGG) were considered as mature free SUMO2/3. Peptides containing but not ending with QQTGG were considered as immature SUMO2 (DVFQQQTGGVY), or immature SUMO3 (DVFQQQTGGSASRGSVPTPNRCP).

Western blotting

3T3-L1 cells were grown as described in "*Adipocyte culture, differentiation and treatment*". Cells were washed with PBS prior lysis in ice-cold RIPA buffer (150 mM NaCl, 50 mM Tris-HCl pH 7.5, 5 mM EDTA, 1 % NP-40, 0.5 % Na-deoxycholate, 0.1 % SDS) freshly supplemented with protease inhibitor (Roche) and 20 mM of NEM. Lysates were sonicated 5 min (30 sec on, 30 sec off) then centrifuged 15 min at 14 000 rpm and 4 °C. To eliminate lipids supernatants were applied to a RNeasy column and centrifuged at 10,000 rpm and 4 °C for 1 min (Qiagen, 74104). The flow through was collected and protein concentrations were assessed using the Bradford assay. 30 µg of proteins were used for each western blot and proteins were detected using anti-SUMO2/3 (ab3742, Abcam) and anti-TBP (ab51841, Abcam) antibodies.

Data analysis

The hierarchical clustering and heatmaps were generated using Perseus software v1.6.10.50 (Tyanova et al., 2016). For SUMO2/3 proteomics, the label-free quantified (LFQ) value for four bio-replicates was averaged. The averaged value was log2 transformed, imputed with default setting, and normalized by row Z score transformation. For SLAM-sequencing data, the normalized count for three bio-replicates was averaged. The averaged normalized count was log2 transformed and normalized by row Z score transformation. The row dendrogram was generated based on Euclidean distance and processed with k-means. Z score was used to generate cluster profiles in parallel.

GO analysis was performed using clusterProfiler R package (Yu et al., 2012). The statistical significance was specified as adjusted p value < 0.05. Redundant GO terms were simplified according to similarity measured with "Wang" method.

The scatter plot was generated using Perseus software. Log2 transformed normalized counts were plotted. Meanwhile, Pearson correlation coefficient and P value were calculated.

Venn diagram was generated using VennDiagram R package (https://CRAN.R-project.org/package=VennDiagram).

For each single gene, Pearson correlation coefficient was calculated by comparing time-course profiles in different datasets in Excel. The density plot for the distribution of Pearson correlation coefficient was generated using EaSeq software v1.111 (Lerdrup et al., 2016).

The ggplot2 R package v3.3.2 (https://ggplot2.tidyverse.org) was used to generate box, histogram, bar, dot and line plots in the study.

Integrative Genomics Viewer (Robinson et al., 2011) was used for SLAM-seq and ChIP-seq data visualization with normalized bigWig files.

Quantification and statistical analysis

Statistical analysis was performed using GraphPad Prism (v7). For immunofluorescence data, Results are presented as mean ± SD. Between groups, statistical significance was calculated using unpaired, two tailed Student's t tests. The significance of mean comparison in boxplots for time course studies was analyzed using stat_compare_means function in R. The paired t-test method was specified. Non-significant: $p > 0.05$, *: $p \leq 0.05$, **: $p \leq 0.01$, ***: $p \leq 0.001$, ****: $p \leq 0.0001$. P values < 0.05 were considered as significant. For overrepresentation analysis, Hypergeometric test was used for testing significance in R. P values were corrected by Benjamini-Hochberg method.

Acknowledgements

This work was supported by EPIC-XS (grant agreement EPIC-XS-823839, project number 0000062) funded by the Horizon 2020 programme of the European Union, a Helse Sør-Øst researcher grant (project number 2017064) and a Norwegian Research Council researcher grant (project number 301268) to PC. The work carried out in the Nielsen lab was in part supported by the Novo Nordisk Foundation Center for Protein Research, the Novo Nordisk Foundation (grant agreement numbers NNF14CC0001 and NNF13OC0006477), Danish Council of Independent Research (grant agreement numbers 4002-00051, 4183-00322A, 8020-00220B and 0135-00096B), and The Danish Cancer Society (grant agreement R146-A9159-16-S2). Sequencing was performed by the GenomEast platform, a member of the 'France Génomique' consortium (ANR-10-INBS-0009). This work was also supported in part by grants from the Norwegian Cancer Society (project number 182524), the Norwegian Research Council (261936) and the Research Council of Norway through its Centers of Excellence funding scheme, project number 262652. We thank Dr. Deo Prakash Panday for fruitful discussions during this project.

Fig. legends

Fig. 1. Characterization of nascent transcriptome dynamics during adipocyte differentiation.

(A) Experimental layout of time-course experiments.

(B and C) Expression profile of time-course transcripts in Quant-seq *(B)* and SLAM-seq *(C)*.

(D and E) Hierarchical clustering of differentially expressed (DE) nascent transcripts (*D*). Clusters are further categorized to 3 stage-specific modules (*E*). PA: pre-adipocyte, CE: clonal expansion, MA: mature adipocyte. Z score is calculated for log2 transformed normalized counts.

(F) Expression profiles of representative nascent transcripts in each transcription module *(E)*.

(G) GO analysis of transcription modules.

Fig. 2. Sumoylation supports adipogenic genes transcription.

(A) Experimental setup of time-course experiments.

(B and C) Effects of ML-792 (log2 fold change) on transcripts across time points in Quant-seq *(B)* and SLAM-seq *(C)*.

(D) GO analysis of SLAM-seq DEGs after ML-792 treatment.

(E) Expression profiles of SLAMseq transcripts (Fig. 1E) in DMSO (colored) and ML-792 (black). Z scores are calculated for log2 transformed normalized counts.

F) Linear relationship (Pearson correlation coefficient) between expression profiles in DMSO and ML-792. Hypothetical pattern effects versus amplitude effects are described in the left and right inserts, respectively.

(G) Representative transcripts of pattern effects (upper panel) and amplitude effects (lower panel).

(H) Effects of ML-792 (log2 fold change) on DE transcripts in fat cell differentiation term and randomly picked population in SLAM-seq. The significance of mean comparison is determined by paired t-test. **: $p \leq 0.01$, ***: $p \leq 0.001$.

Fig. 3. A dual role for SUMO at the chromatin.

(A) Experimental setup of time course experiment.

(B) Heatmap of SUMO occupancy within a 10 kb window centered on SUMO peak summit. SUMO peaks are sorted by increasing size. The intensity represents log10 transformed FPKM.

(C and D) Hierarchical clustering of SUMO peaks during AD (*C*). Clusters are categorized to 3 modules: PA, CE and MA (*D*). Z scores are calculated for log2 transformed normalized counts.

(E) GO analysis of SUMO target genes in PA, CE and A modules.

(F) Heatmap of SLAMseq AD clusters (see Fig. 1E) and corresponding SUMO peaks. Pearson correlation coefficients between transcription levels and SUMO occupancy of genes are indicated by gradient color.

(G) Heatmap of SUMO occupancy within 10 kb window centered on SUMO summits. SUMO peaks are sorted in the same order as *(F)*. The intensity represents log10 transformed FPKM.

(H and I) Distributions of Pearson correlation coefficients in *(F)* in groups categorized base on genomic locations of SUMO peaks *(H)* and in three AD modules *(I)*. All: all SUMO peaks, P: promoter-TSS, E: exon, I: intron, DP: distant promoter. The y axis is segmented into 10 bins.

(J and K) Profiles (Loess regression lines) of SLAMseq (CTRL, blue; ML-792, yellow) and SUMO ChIPseq (Black) for up-regulated genes *(J, correppression)* and down-regulated genes *(K, coactivation)* upon ML-792 treatment.

(L) Motif enrichment of SUMO binding at TFBSs during AD.

(M) SUMO, Pparγ and RXR ChIPseq signals during AD.

Fig. 4. Site specific characterization of the endogenous SUMOylome of differentiating adipocytes.

(A) Schematic overview of endogenous SUMO2/3 proteomics.

(B) Quantification of total SUMO2/3 density.

(C) SUMO equilibrium.

(D-E) Hierarchical clustering of sumoylated proteins (*D*). Clusters are categorized in 3 modules: PA, CE and MA (*E*).

(F) GO analysis of sumoylation modules.

(G) Heat maps of SUMO, Pparγ and RXR peaks at the 208 Pparγ/RXR target genes differentially expressed during AD. Order of rows is the same as in *(H)*.

(H) Hierarchical clustering of DE nascent transcripts of the 208 Pparγ/RXR target genes in *(G)*. Z score is calculated for log2 transformed normalized counts.

(I) Global downregulation of 208 Pparγ/RXR target genes transcription in MA upon ML-792 treatment.

Fig. S1. Transcriptomic characterization of differentiating adipocytes.

(A) Schematic overview of 3T3-L1 treatment with DMSO and ML-792 over time.

(B) Immunofluorescence analysis of DMSO or ML-792 treated adipocytes (Day 7). Lipid droplets were stained with lipid probe Bodipy. Nucleus was counterstained with DAPI. Images were acquired using the ImageXpress Micro Confocal device (40x). Images are representative of at least 3 biological replicates.

(C) The size of lipid droplets in DMSO or ML-792 treated adipocytes (Day 7) was measured using FIJI software. The surface area is measured in μm^2 (y axis). At least 4 representative fields per well were analyzed. The significance of mean comparison is determined by unpaired t-test. ns: $p > 0.05$, *: $p \leq 0.05$, **: $p \leq 0.01$, ***: $p \leq 0.001$, ****: $p \leq 0.0001$.

(D) The percentage of adipocytes (y axis) in subpopulations categorized based on lipid droplet numbers per cell (x axis).

(E) PCA of QuantSeq data.

(F) Table describing the number of DE transcripts or genes in QuantSeq and SLAMseq.

(G and H) Hierarchical clustering of time-course DE transcripts in QuantSeq (*G*). Clusters are further categorized to 3 modules (*H*). Z score is calculated for log2 transformed normalized counts.

(I) GO analysis of QuantSeq modules.

(J) Expression profiles, represented as normalized counts, of representative transcripts in modules in QuantSeq.

(K) PCA of SLAMseq data.

(L) Venn diagram featuring QuantSeq and SLAMseq common DEGs.

(M) Expression profile of common QuantSeq and SLAMseq AD transcripts.

(N) Contrary to *CEBPA*, *CEBPB* and *CEBPD* display opposite expression profiles between QuantSeq and SLAMseq.

Fig. S2. ML-792 affects adipogenesis transcription modules.

(A) Fat cell differentiation term enrichment among SLAMseq AD DEGs, ML-792 DEGs and common AD and ML-792 DEGs.

(B) Heatmap showing 927 common DE transcripts in the AD clusters (Fig. 1E). CTRL: DMSO.

(C and D) Distributions of Pearson correlation coefficients in transcription modules. P: pattern effect, A: amplitude effect. Y axis in *(C)* is represented as transcript count numbers. The y axis is segmented into 10 bins.

(E) Effects of ML-792 (log2 fold change) on DE transcripts in fat cell differentiation term in QuantSeq and SLAMseq. *: $p \leq 0.05$, **: $p \leq 0.01$, ***: $p \leq 0.001$.

Fig. S3. SUMO promotes transcription of adipogenic gene.

(A) PCA of SUMO ChIP-seq data.

(B) Genome-wide distribution of SUMO peaks.

(C) GO analysis of genes closest to the SUMO peaks that are differentially regulated during adipogenesis.

(D) Genome browser snapshots of ChIPseq and SLAMseq data at *KLF10* (negative correlation) and *FABP4* (positive correlation).

(E) Hierarchical clustering of AD SLAMseq transcripts in DMSO (Fig 1E) and ML-792 with SUMO ChIPseq during AD. Log2 fold change between ML-792 and DMSO treatments were calculated.

(F) GO analysis of genes at which SUMO acts as corepressor (CoR) and coactivator (CoA).

(G) Bimodal test of TFBS enrichment across time points as observed in Fig. 3L.

(H) Motif enrichment of SUMO binding at TFBSs of SLAMseq DEGs *(F* and *G)*.

Fig. S4. Site specific characterization of the endogenous SUMOylome of differentiating adipocytes.

(A) Pearson correlation analysis of MS bioreplicates.

(B) PCA of site-specific sumoylation across samples.

(C) Western blot analysis of sumoylation levels at day -2 and day 7. Loading control: TATA Binding Protein (TBP).

(D) PCA of SUMO targets.

(E) GO analysis of SUMO targets.

(F) Venn diagram of SUMO targets identified in this study and two recently published studies that used endogeneous detection of sumoylated sites.

(G) Metascape analysis of the top 100 SUMO targets from the studies in *(F)*.

(H) Sumoylation profiles of representative SUMO targets of AD sumoylation modules in 4Fig. D and E.

(I) GO analysis of Pparγ, RXR, SUMO targets.

(J) Loess regression lines of SLAMseq dynamics (CTRL, blue; ML-792, yellow), SUMO ChIPseq intensity at PPRE (red) and SUMOylated Pparγ (green) and RXR (Turquoise) at 208 Pparγ target genes in Figure 4G-I. Z scores are calculated for log2 transformed normalized counts transcript or SUMO site) or log2 transformed label-free quantified (LFQ) values (SUMO proteomics).

(K) Snapshot of IGV genome browser showing the activation of the Pparγ/RXR target gene *SCD1* during AD (SLAMseq, DMSO), the downregulation of *SCD1* after ML-792 treatment (SLAMseq, ML-792) and the coordinated recruitment of SUMO, Pparγ and RXR at *SCD1* during AD (ChIPseq).

References

Amemiya, H.M., Kundaje, A., and Boyle, A.P. (2019). The ENCODE Blacklist: Identification of Problematic Regions of the Genome. Sci Rep *9*, 9354.

Anders, S., and Huber, W. (2010). Differential expression analysis for sequence count data. Genome biology *11*, R106.

Baik, H., Boulanger, M., Hosseini, M., Kowalczyk, J., Zaghdoudi, S., Salem, T., Sarry, J.E., Hicheri, Y., Cartron, G., Piechaczyk, M., et al. (2018). Targeting the SUMO Pathway Primes All-trans Retinoic Acid-Induced Differentiation of Nonpromyelocytic Acute Myeloid Leukemias. Cancer Res *78*, 2601-2613.

Benjamini, Y., and Hochberg, Y. (1995). Controlling the False Discovery Rate: A Practical and Powerful Approach to Multiple Testing. Journal of the Royal Statistical Society. Series B (Methodological) *57*, 289-300.

Chung, S.S., Ahn, B.Y., Kim, M., Choi, H.H., Park, H.S., Kang, S., Park, S.G., Kim, Y.B., Cho, Y.M., Lee, H.K., et al. (2010). Control of adipogenesis by the SUMO-specific protease SENP2. Mol Cell Biol *30*, 2135-2146.

Chymkowitch, P., Nguea, A.P., Aanes, H., Koehler, C.J., Thiede, B., Lorenz, S., Meza-Zepeda, L.A., Klungland, A., and Enserink, J.M. (2015a). Sumoylation of Rap1 mediates the recruitment of TFIID to promote transcription of ribosomal protein genes. Genome Res *25*, 897-906.

Chymkowitch, P., Nguea, P.A., Aanes, H., Robertson, J., Klungland, A., and Enserink, J.M. (2017). TORC1-dependent sumoylation of Rpc82 promotes RNA polymerase III assembly and activity. Proc Natl Acad Sci U S A *114*, 1039-1044.

Chymkowitch, P., Nguea, P.A., and Enserink, J.M. (2015b). SUMO-regulated transcription: challenging the dogma. Bioessays *37*, 1095-1105.

Cignarelli, A., Melchiorre, M., Peschechera, A., Conserva, A., Renna, L.A., Miccoli, S., Natalicchio, A., Perrini, S., Laviola, L., and Giorgino, F. (2010). Role of UBC9 in the regulation of the adipogenic program in 3T3-L1 adipocytes. Endocrinology *151*, 5255-5266.

Colitti, M., Boschi, F., and Montanari, T. (2018). Dynamic of lipid droplets and gene expression in response to beta-aminoisobutyric acid treatment on 3T3-L1 cells. Eur J Histochem *62*.

Cossec, J.C., Theurillat, I., Chica, C., Bua Aguin, S., Gaume, X., Andrieux, A., Iturbide, A., Jouvion, G., Li, H., Bossis, G., et al. (2018). SUMO Safeguards Somatic and Pluripotent Cell Identities by Enforcing Distinct Chromatin States. Cell Stem Cell *23*, 742-757 e748.

Cox, A.R., Chernis, N., Kim, K.H., Masschelin, P.M., Saha, P.K., Briley, S.M., Sharp, R., Felix, J.B., Moore, D.D., Pangas, S.A., et al. (2020). Ubc9 deletion in adipocytes causes lipoatrophy in mice. bioRxiv, 2020.2009.2012.294629.

Cox, J., and Mann, M. (2008). MaxQuant enables high peptide identification rates, individualized p.p.b.-range mass accuracies and proteome-wide protein quantification. Nat. Biotechnol *26*, 1367-1372.

Cox, J., Neuhauser, N., Michalski, A., Scheltema, R.A., Olsen, J.V., and Mann, M. (2011). Andromeda: a peptide search engine integrated into the MaxQuant environment. J. Proteome. Res *10*, 1794-1805.

Decque, A., Joffre, O., Magalhaes, J.G., Cossec, J.C., Blecher-Gonen, R., Lapaquette, P., Silvin, A., Manel, N., Joubert, P.E., Seeler, J.S., et al. (2016). Sumoylation coordinates the repression of inflammatory and anti-viral gene-expression programs during innate sensing. Nat Immunol *17*, 140-149.

Enserink, J.M. (2015). Sumo and the cellular stress response. Cell Div *10*, 4.
Garcia-Nino, W.R., and Zazueta, C. (2021). New insights of Kruppel-like transcription factors in adipogenesis and the role of their regulatory neighbors. Life Sci *265*, 118763.
He, X., Riceberg, J., Soucy, T., Koenig, E., Minissale, J., Gallery, M., Bernard, H., Yang, X., Liao, H., Rabino, C., et al. (2017). Probing the roles of SUMOylation in cancer cell biology by using a selective SAE inhibitor. Nat Chem Biol *13*, 1164-1171.
Heinz, S., Benner, C., Spann, N., Bertolino, E., Lin, Y.C., Laslo, P., Cheng, J.X., Murre, C., Singh, H., and Glass, C.K. (2010). Simple combinations of lineage-determining transcription factors prime cis-regulatory elements required for macrophage and B cell identities. Molecular cell *38*, 576-589.
Hendriks, I.A., Lyon, D., Su, D., Skotte, N.H., Daniel, J.A., Jensen, L.J., and Nielsen, M.L. (2018). Site-specific characterization of endogenous SUMOylation across species and organs. Nat Commun *9*, 2456.
Hendriks, I.A., and Vertegaal, A.C. (2016). A comprehensive compilation of SUMO proteomics. Nat Rev Mol Cell Biol *17*, 581-595.
Herzog, V.A., Reichholf, B., Neumann, T., Rescheneder, P., Bhat, P., Burkard, T.R., Wlotzka, W., von Haeseler, A., Zuber, J., and Ameres, S.L. (2017). Thiol-linked alkylation of RNA to assess expression dynamics. Nature methods *14*, 1198-1204.
Kharchenko, P.V., Tolstorukov, M.Y., and Park, P.J. (2008). Design and analysis of ChIP-seq experiments for DNA-binding proteins. Nat Biotechnol *26*, 1351-1359.
Langmead, B. (2010). Aligning short sequencing reads with Bowtie. Curr Protoc Bioinformatics *Chapter 11*, Unit 11 17.
Lefterova, M.I., Haakonsson, A.K., Lazar, M.A., and Mandrup, S. (2014). PPARgamma and the global map of adipogenesis and beyond. Trends Endocrinol Metab *25*, 293-302.
Lerdrup, M., Johansen, J.V., Agrawal-Singh, S., and Hansen, K. (2016). An interactive environment for agile analysis and visualization of ChIP-sequencing data. Nat Struct Mol Biol *23*, 349-357.
Liu, B., Wang, T., Mei, W., Li, D., Cai, R., Zuo, Y., and Cheng, J. (2014). Small ubiquitin-like modifier (SUMO) protein-specific protease 1 de-SUMOylates Sharp-1 protein and controls adipocyte differentiation. J Biol Chem *289*, 22358-22364.
Love, M.I., Huber, W., and Anders, S. (2014). Moderated estimation of fold change and dispersion for RNA-seq data with DESeq2. Genome biology *15*, 550.
Mikkonen, L., Hirvonen, J., and Janne, O.A. (2013). SUMO-1 regulates body weight and adipogenesis via PPARgamma in male and female mice. Endocrinology *154*, 698-708.
Neyret-Kahn, H., Benhamed, M., Ye, T., Le Gras, S., Cossec, J.C., Lapaquette, P., Bischof, O., Ouspenskaia, M., Dasso, M., Seeler, J., et al. (2013). Sumoylation at chromatin governs coordinated repression of a transcriptional program essential for cell growth and proliferation. Genome Res *23*, 1563-1579.
Nguea, P.A., Robertson, J., Herrera, M.C., Chymkowitch, P., and Enserink, J.M. (2019). Desumoylation of RNA polymerase III lies at the core of the Sumo stress response in yeast. J Biol Chem *294*, 18784-18795.
Nielsen, R., Pedersen, T.A., Hagenbeek, D., Moulos, P., Siersbaek, R., Megens, E., Denissov, S., Borgesen, M., Francoijs, K.J., Mandrup, S., et al. (2008). Genome-wide profiling of PPARgamma:RXR and RNA polymerase II occupancy reveals temporal activation of distinct metabolic pathways and changes in RXR dimer composition during adipogenesis. Genes Dev *22*, 2953-2967.

Niskanen, E.A., Malinen, M., Sutinen, P., Toropainen, S., Paakinaho, V., Vihervaara, A., Joutsen, J., Kaikkonen, M.U., Sistonen, L., and Palvimo, J.J. (2015). Global SUMOylation on active chromatin is an acute heat stress response restricting transcription. Genome biology *16*, 153.
Psakhye, I., and Jentsch, S. (2012). Protein group modification and synergy in the SUMO pathway as exemplified in DNA repair. Cell *151*, 807-820.
Quinlan, A.R., and Hall, I.M. (2010). BEDTools: a flexible suite of utilities for comparing genomic features. Bioinformatics *26*, 841-842.
Rappsilber, J., Ishihama, Y., and Mann, M. (2003). Stop and go extraction tips for matrix-assisted laser desorption/ionization, nanoelectrospray, and LC/MS sample pretreatment in proteomics. Anal. Chem *75*, 663-670.
Robinson, J.T., Thorvaldsdottir, H., Winckler, W., Guttman, M., Lander, E.S., Getz, G., and Mesirov, J.P. (2011). Integrative genomics viewer. Nat Biotechnol *29*, 24-26.
Seeler, J.S., and Dejean, A. (2017). SUMO and the robustness of cancer. Nat Rev Cancer *17*, 184-197.
Shah, A., Oldenburg, A., and Collas, P. (2014). A hyper-dynamic nature of bivalent promoter states underlies coordinated developmental gene expression modules. BMC genomics *15*, 1186.
Theurillat, I., Hendriks, I.A., Cossec, J.C., Andrieux, A., Nielsen, M.L., and Dejean, A. (2020). Extensive SUMO Modification of Repressive Chromatin Factors Distinguishes Pluripotent from Somatic Cells. Cell reports *32*, 108146.
Tyanova, S., Temu, T., Sinitcyn, P., Carlson, A., Hein, M.Y., Geiger, T., Mann, M., and Cox, J. (2016). The Perseus computational platform for comprehensive analysis of (prote)omics data. Nature methods.
Yu, G., Wang, L.G., Han, Y., and He, Q.Y. (2012). clusterProfiler: an R package for comparing biological themes among gene clusters. OMICS *16*, 284-287.
Zheng, Q., Cao, Y., Chen, Y., Wang, J., Fan, Q., Huang, X., Wang, Y., Wang, T., Wang, X., Ma, J., et al. (2018). Senp2 regulates adipose lipid storage by de-SUMOylation of Setdb1. J Mol Cell Biol *10*, 258-266.

Figure 1_Zhao et al

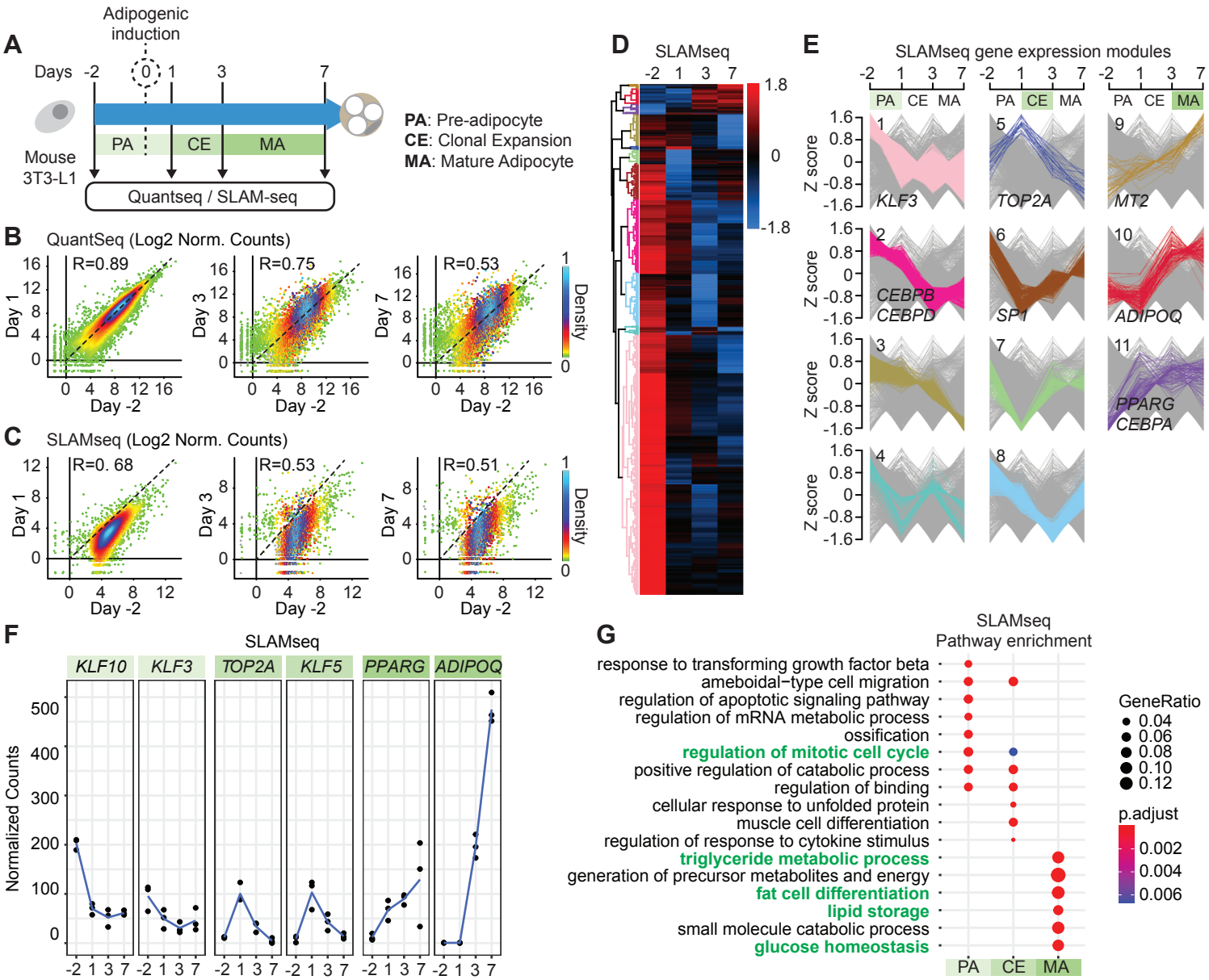

Figure 2_Zhao et al

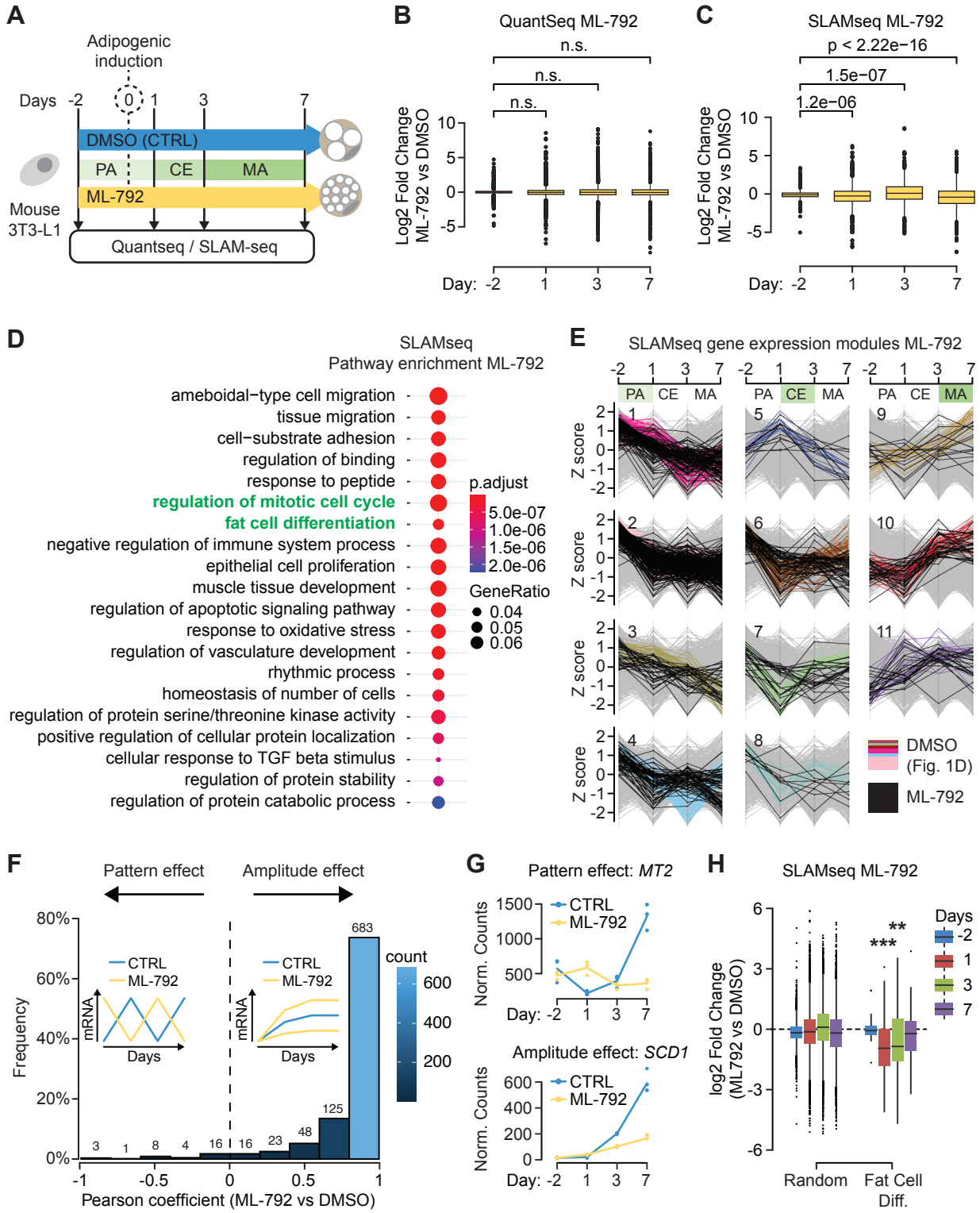

Figure 3_Zhao et al

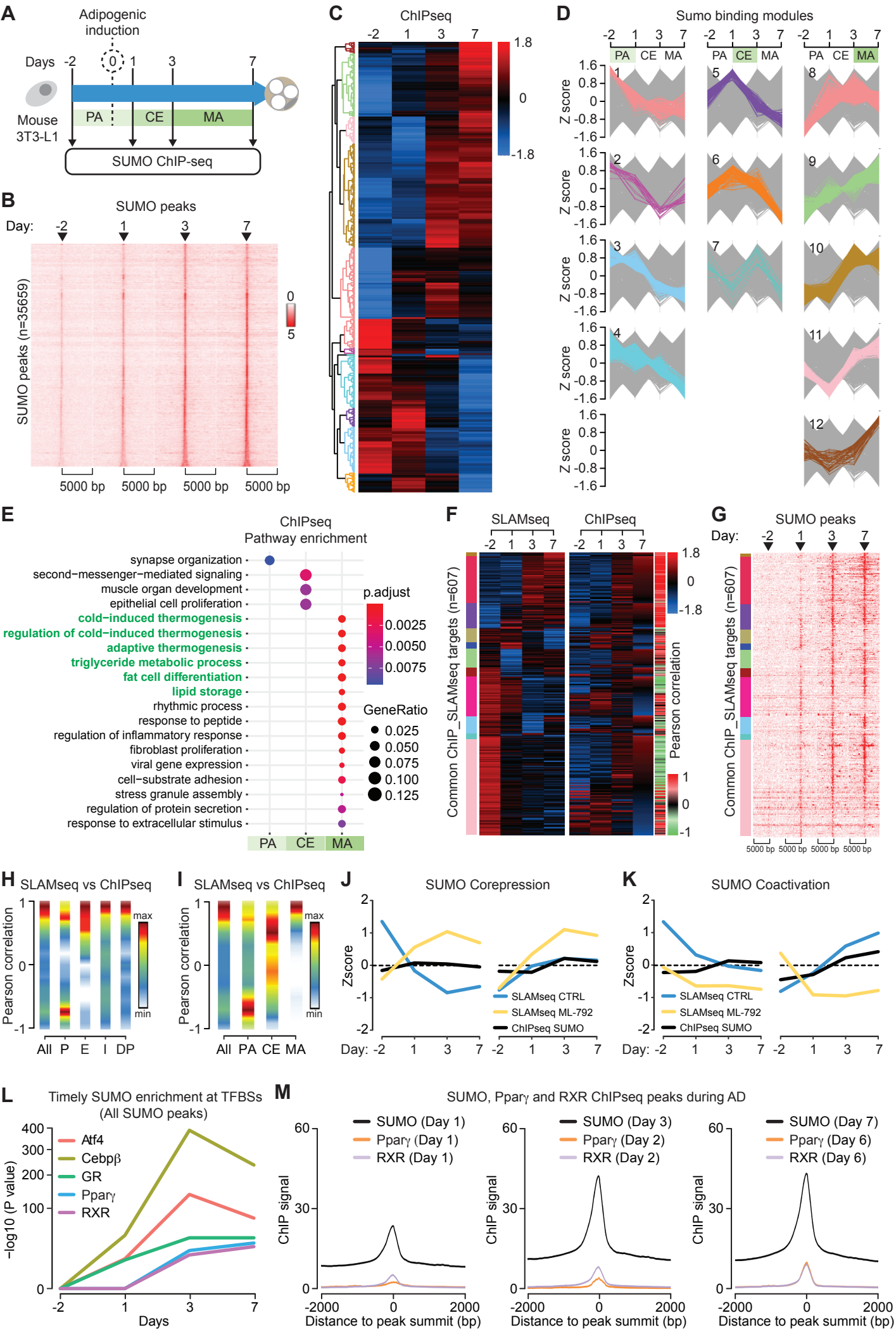

Figure 4_Zhao et al

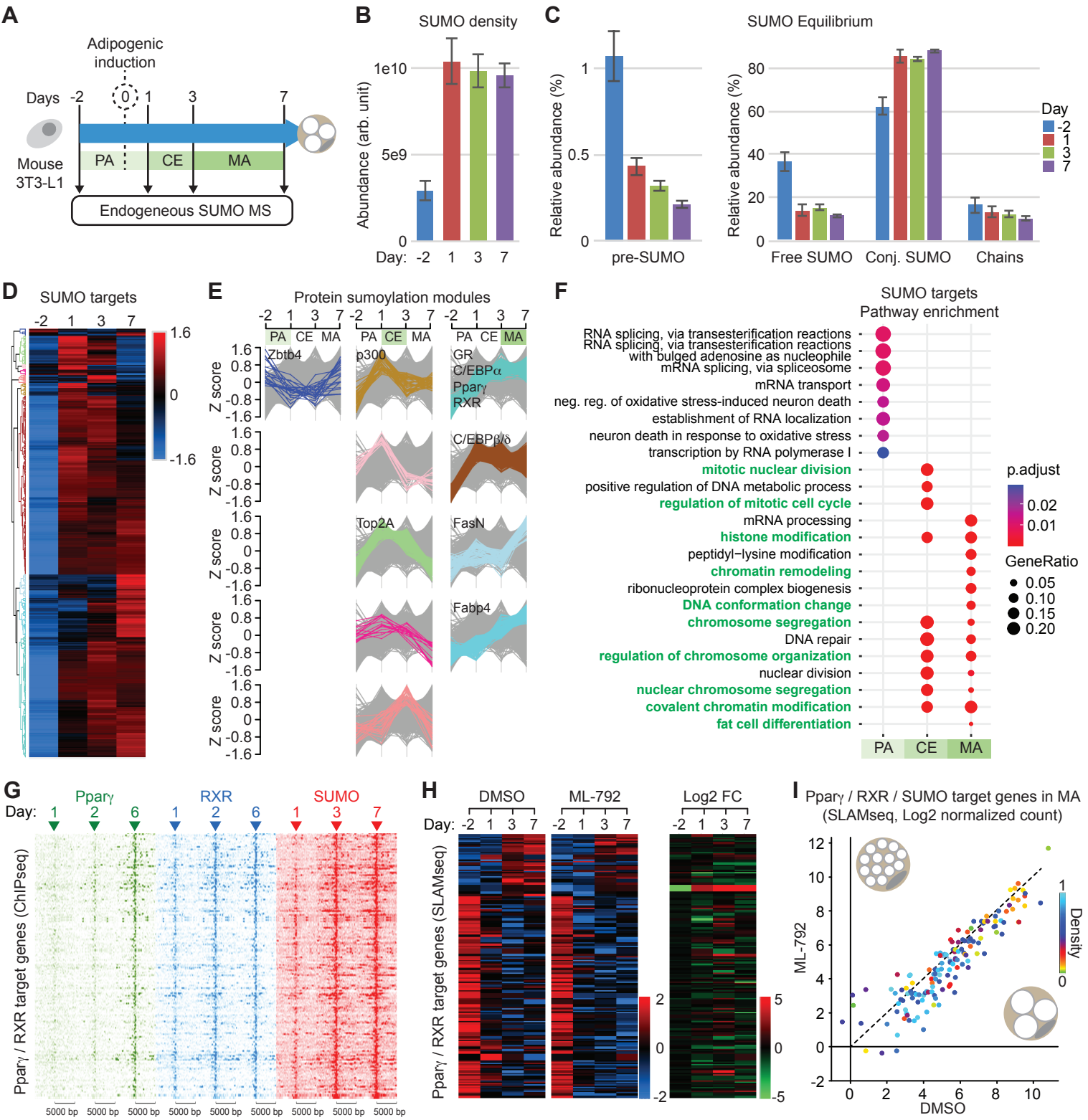

Figure S1_Zhao et al

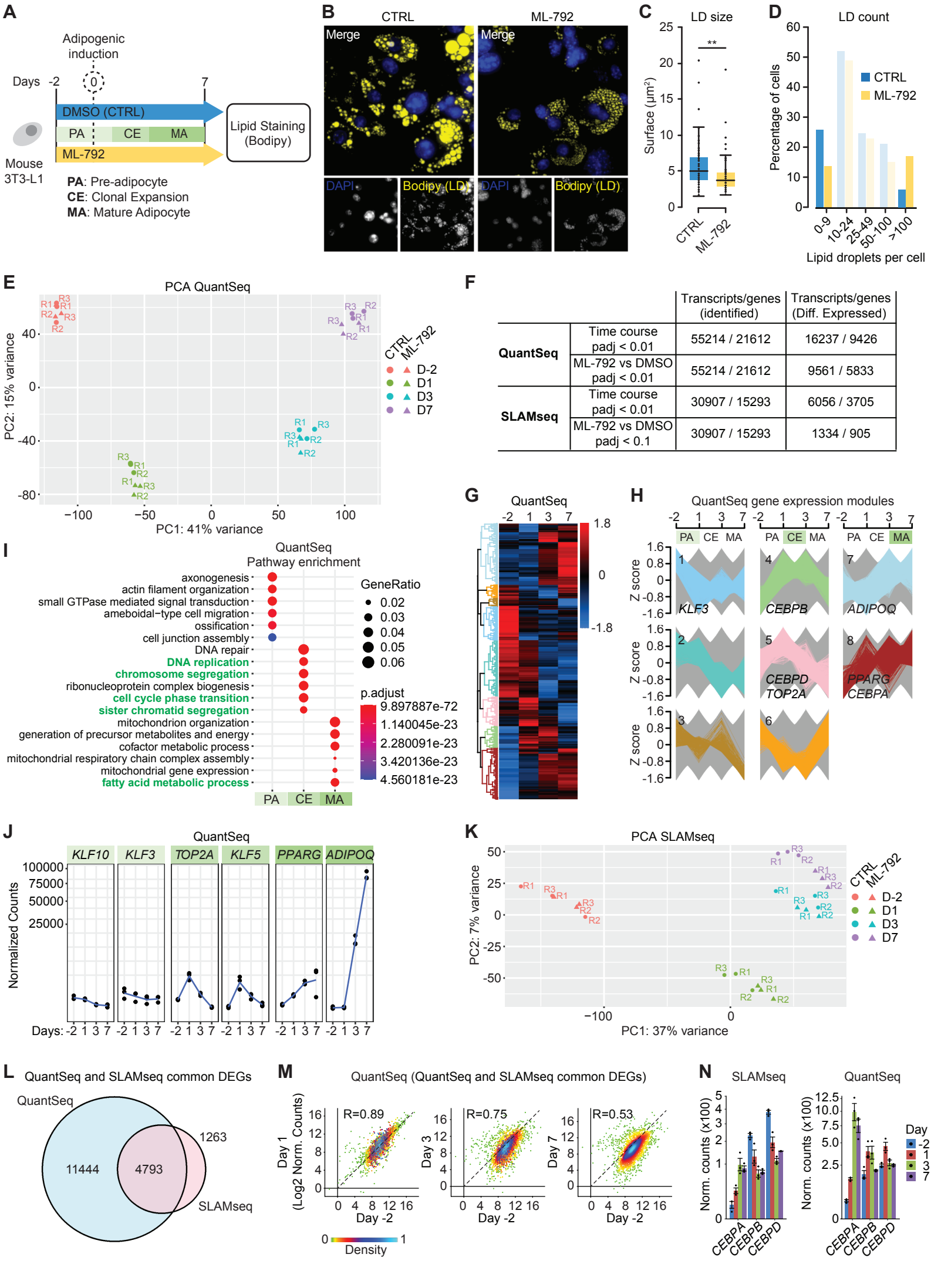

Figure S2_Zhao et al

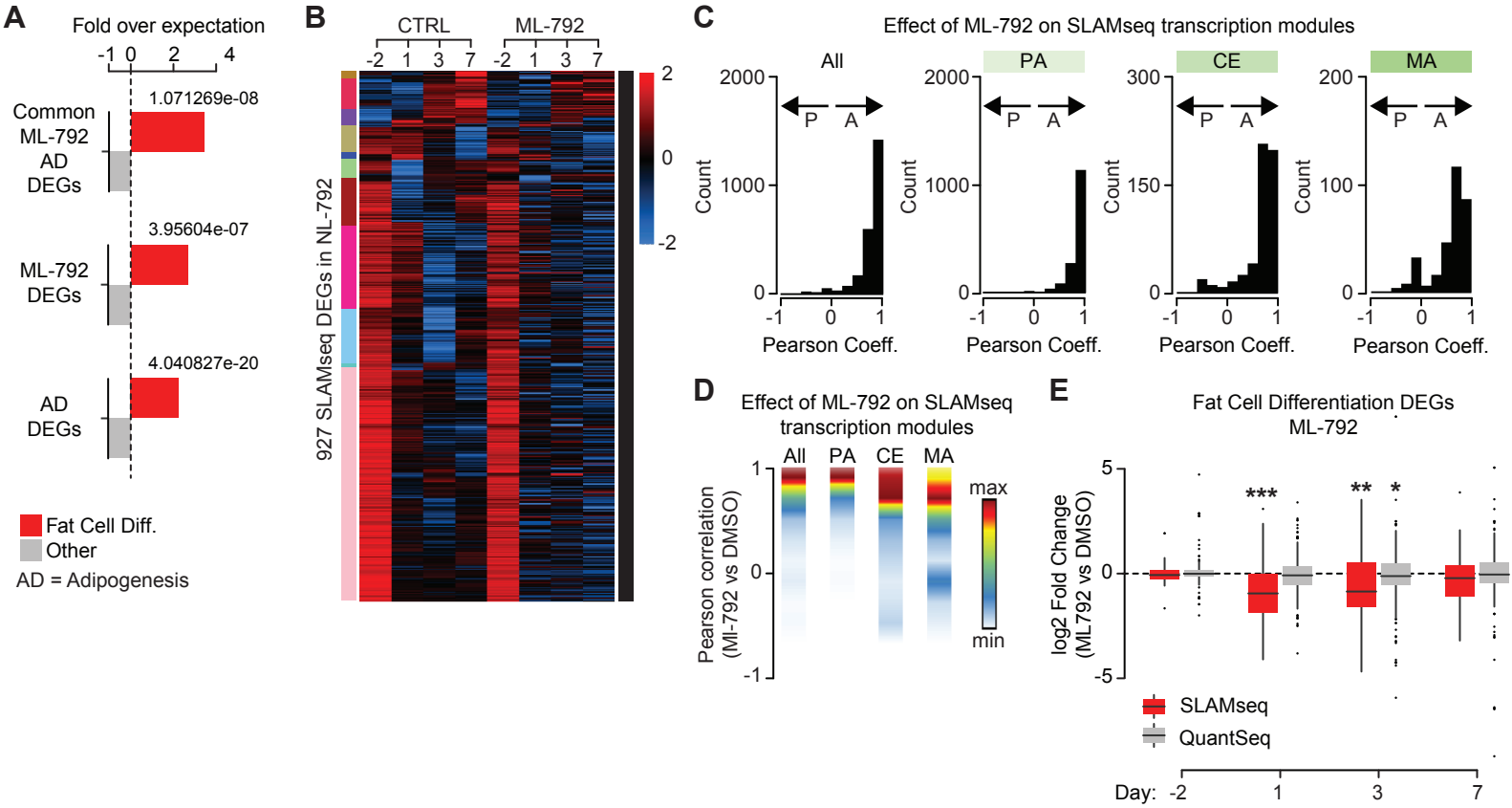

Figure S3_Zhao et al

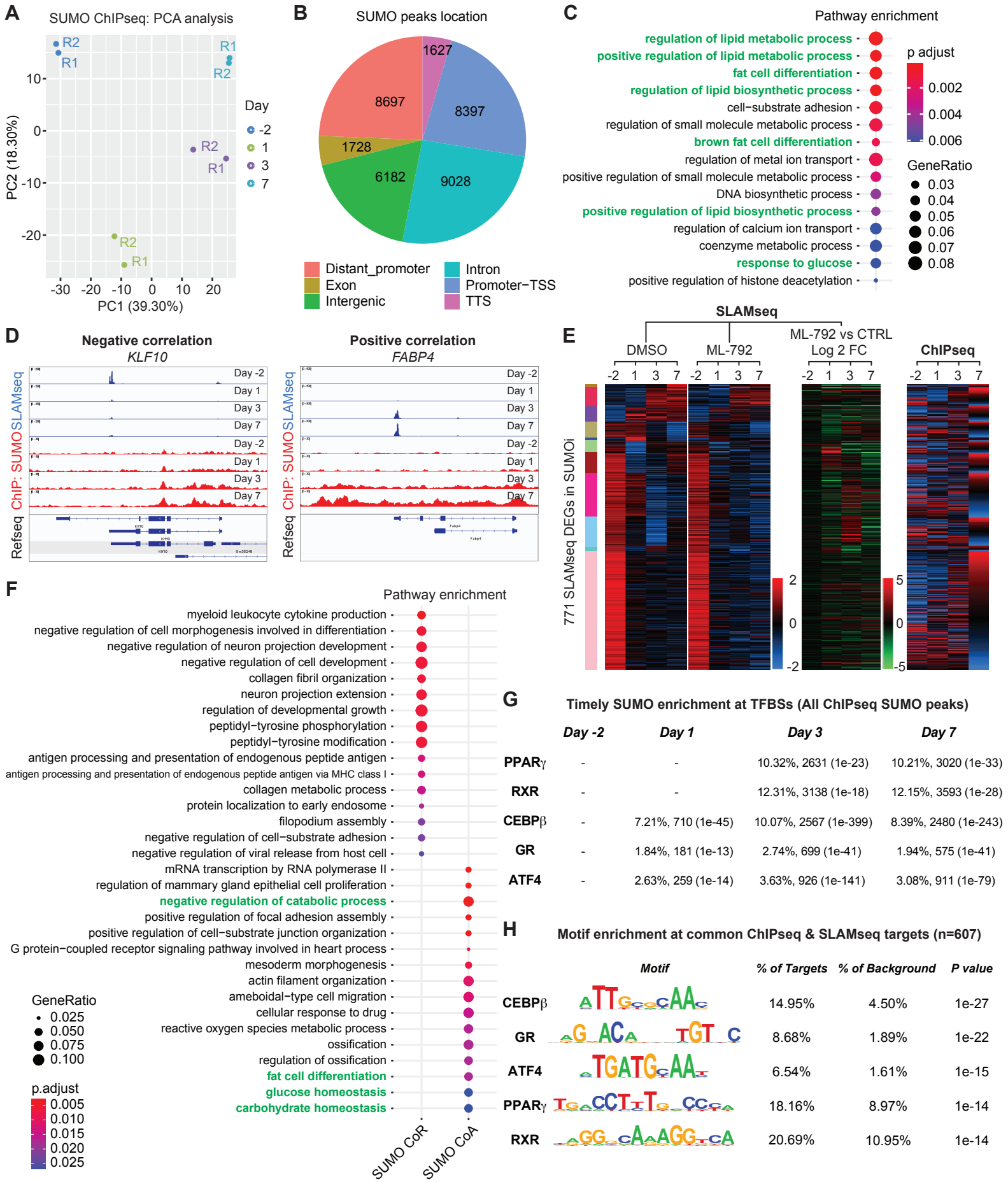

G Timely SUMO enrichment at TFBSs (All ChIPseq SUMO peaks)

	Day -2	*Day 1*	*Day 3*	*Day 7*
PPARγ	-	-	10.32%, 2631 (1e-23)	10.21%, 3020 (1e-33)
RXR	-	-	12.31%, 3138 (1e-18)	12.15%, 3593 (1e-28)
CEBPβ	-	7.21%, 710 (1e-45)	10.07%, 2567 (1e-399)	8.39%, 2480 (1e-243)
GR	-	1.84%, 181 (1e-13)	2.74%, 699 (1e-41)	1.94%, 575 (1e-41)
ATF4	-	2.63%, 259 (1e-14)	3.63%, 926 (1e-141)	3.08%, 911 (1e-79)

H Motif enrichment at common ChIPseq & SLAMseq targets (n=607)

	Motif	*% of Targets*	*% of Background*	*P value*
CEBPβ		14.95%	4.50%	1e-27
GR		8.68%	1.89%	1e-22
ATF4		6.54%	1.61%	1e-15
PPARγ		18.16%	8.97%	1e-14
RXR		20.69%	10.95%	1e-14
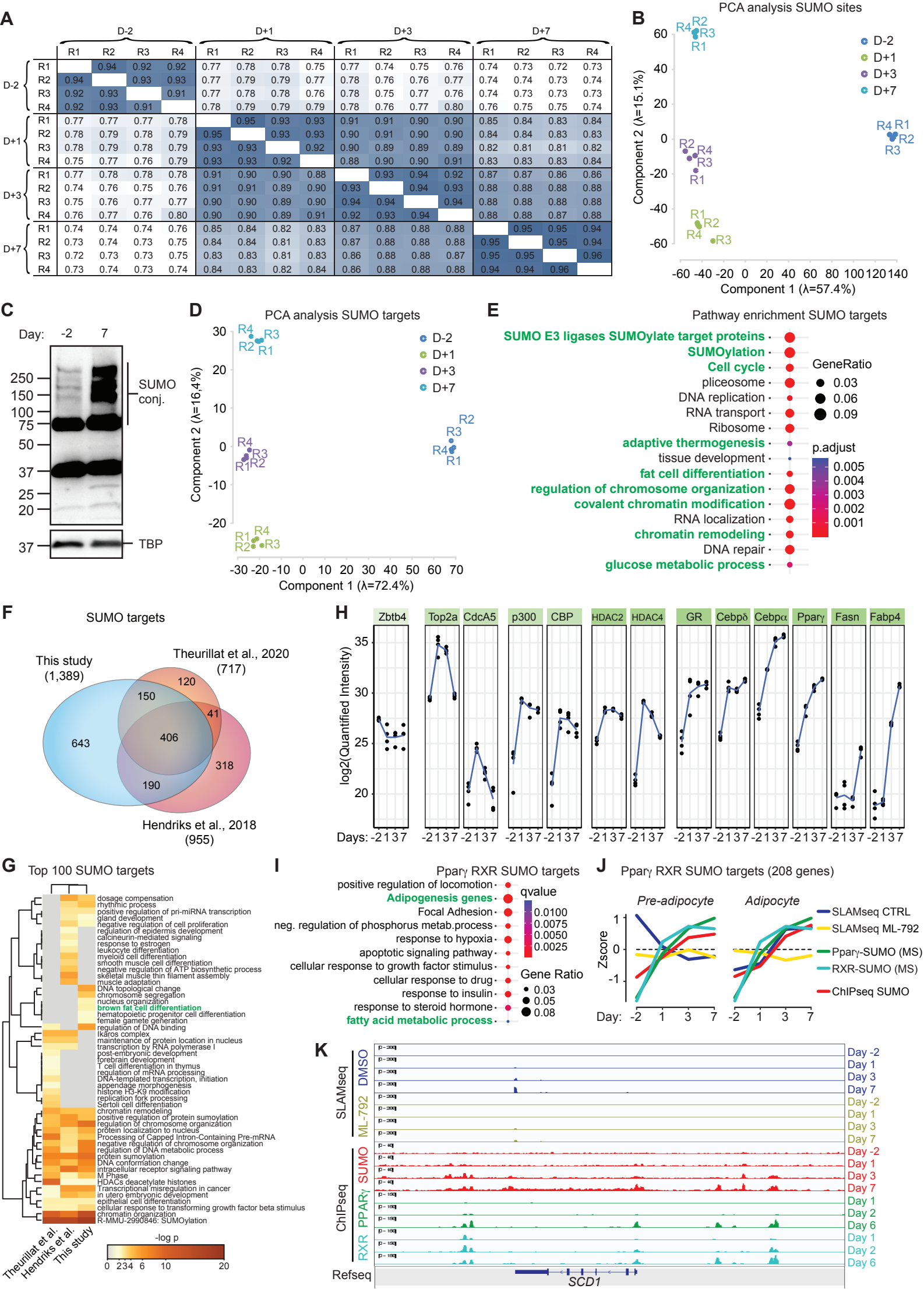
Figure S4_Zhao et al